

Combination Neutron Experiment for Remote Analysis

Neutron techniques can provide chemical analysis of
lunar and planetary surfaces.

R. L. Caldwell, W. R. Mills, Jr.,
L. S. Allen, P. R. Bell, R. L. Heath

One of the objectives of space missions is the remote analysis of lunar and planetary surfaces from which it may be difficult or impossible to collect samples. Nuclear analysis techniques can provide information on the chemical composition and density of rocks which can then be compared with the predictions of the various hypotheses of the origin and evolution of the moon and planets. In this article we describe an experiment based on a combination of four techniques of neutron analysis, the results of which should yield information about some of the important characteristics of the lunar and planetary surfaces.

Neutron methods, basically, measure the elemental composition of material. Therefore, in order to study the capabilities of these methods for analysis of the lunar surface, for instance, one needs estimates of elemental compositions that would be consistent with various hypotheses of the moon's origin. Such estimates have been given by Palm and Strom (1). In order to test the various hypotheses, which are founded primarily either on impact or on volcanic activity, it is sufficient to classify rocks into three types—acidic, basal-

tic, and aerolitic. Table 1, taken from Palm and Strom, shows the expected concentrations of elements for the three types. Any one of these three might exist in both maria and terrae, and analysis of the rock in these regions should make it possible to decide in favor of one of the hypotheses. (For further geological details, see 1.) Determination of the presence of hydrogen, presumably in the form of water, is also of prime importance and can be accomplished by two of the neutron techniques described in this article. In addition, one of the techniques can give some indication of near-surface layering if it exists.

Description of the Method

Neutron-analysis methods utilize the spectral or temporal characteristics, or both, of gamma rays produced when neutrons interact with matter. The radiations are classified as prompt, capture, and activation gamma rays. Prompt gamma rays result from the inelastic scattering of fast neutrons and have discrete energies characteristic of the scattering nuclei. Capture gamma rays arise from the decay of excited energy levels of a nucleus after the capture of a neutron by a parent nucleus; the capture radiation is characteristic of the compound nucleus.

Activation gamma rays arise as a result of fast neutron reactions [for example, (n,p) , (n,α) , $(n,2n)$] or capture of thermal neutrons. The unstable nuclei thus formed decay by emitting beta particles and gamma rays. The characteristic half-life of these nuclei is usually greater than a few seconds and should be not more than a few hours if the emissions are to be of use in the application discussed here. With a pulsed neutron source, activation analysis could be readily performed in the usual way or by cyclical counting of the activation gamma rays in a time interval after the capture gamma rays have died away and before the next neutron burst. This repetitive counting appears to have some advantages over conventional activation counting techniques, as we shall show.

The use of a combination of several neutron reactions for analysis of composition has been previously discussed by Monaghan *et al.* (2) and by Trombka and Metzger (3). These authors give a general discussion of the requirements of an instrument for neutron analysis. Trombka and Metzger also give results of investigations performed at such laboratories as the Lawrence Radiation Laboratory (4), the Activation Analysis Research Laboratory of the A&M College of Texas (5), the Jet Propulsion Laboratory (3), and the Armour Research Foundation (now Illinois Institute of Technology Research Institute) (6).

In addition to measuring the energy of prompt and capture gamma rays and the energy and half-life of activation gamma rays, one can analyze materials by measuring the rate at which thermal neutrons die away after a burst of fast neutrons (7). A time analysis of the decay of the capture gamma rays is a convenient way of following the neutron die-away (8). These four measurements (prompt, capture, die-away, and activation) constitute an improved combination method of neutron analysis which can be performed with a single instrument. The basic requirements for the instrument are a scintillation crystal detector, a miniature ac-

Drs. Caldwell, Mills, and Allen are on the staff of the Field Research Laboratory of Socony Mobil Oil Company, Inc., Dallas, Texas. Dr. Bell is at the Oak Ridge National Laboratory, Oak Ridge, Tennessee. Dr. Heath is at the National Reactor Testing Station, Idaho Falls, Idaho.

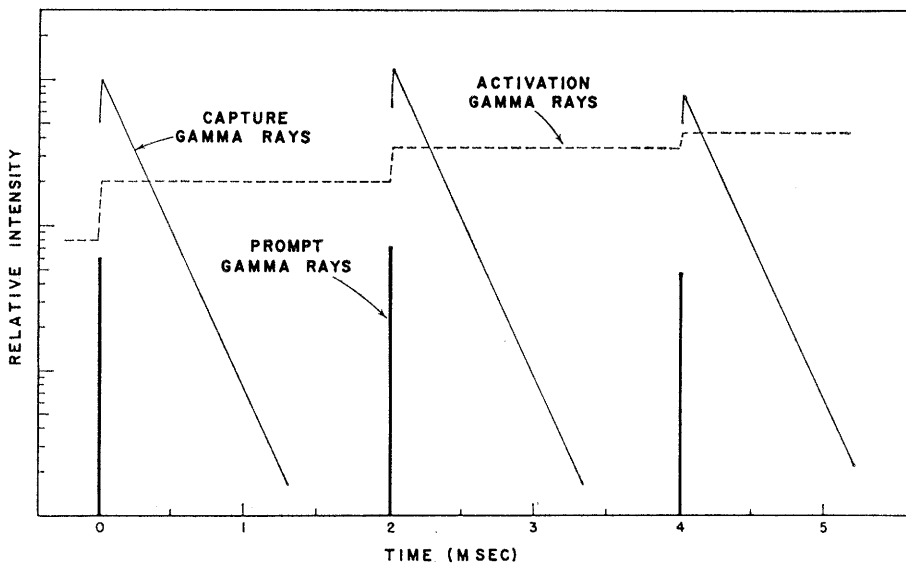


Fig. 1. Timing diagram for combination neutron experiment.

celerator neutron source which can be pulsed, a multichannel analyzer with pulse-height and time-analysis modes, and a programmer to control the overall experiment. In addition, before the neutron source is turned on, the natural gamma-ray background should be measured to obtain further information about the nature of the surface material.

The three types of gamma rays may be separated on the basis of their time and energy distributions. Figure 1 illustrates schematically how these gamma rays behave as a function of time when the neutron source is pulsed. We have assumed that fast neutrons are produced by a neutron source in 20-microsecond bursts at a rate of 500 per second. Three successive bursts are shown with output varying by ± 20 percent. Prompt gamma rays (from inelastic scattering) appear only during the bursts. The intensity of the capture gamma rays is proportional to the density of slow or thermal neutrons and builds up during and dies away after each burst. This behavior is characterized by the exponential $e^{-\lambda t}$, where λ is the decay constant and t is the time during any source cycle measured from the beginning of the burst. For the case shown, we have arbitrarily chosen λ^{-1} to be 200 microseconds, a typical value. We have assumed that the activation gamma rays are produced as a result of a fast neutron reaction and that the mean life of the activity is 1 second. The time behavior is characterized by e^{-t} , where t is measured in seconds. On the time scale used in Fig. 1, the build-up dur-

ing the burst is linear and the decay between bursts is unobservable. An arbitrary background level has been assumed at time zero. An important feature of the time pattern is that the intensities of prompt gamma rays and capture gamma rays from successive bursts are independent, whereas the intensity of activation gamma rays is cumulative. After the last burst, the decay of activation gamma rays will be proportional to e^{-t} .

Figure 2 shows the spectral features of the three types of radiation obtained from the five elements expected to be most abundant in the lunar surface. The heights of the bars for a given element are proportional to $\sigma\Gamma$, where σ is the cross section for the appropriate process and Γ is the number of gamma rays of a given energy which are produced per interaction. Thus the intensities of different lines for a given element are correctly normalized for comparison (by assuming equal fast and slow neutron fluxes), but intensities are not properly normalized from element to element.

From Fig. 2 it can be seen how a qualitative analysis of the elements may be performed by observing separately the energy spectra of prompt, capture, and activation gamma rays, by using time discrimination based on Fig. 1. Oxygen may be identified on the basis of the high-energy prompt gamma rays. Magnesium is characterized by a 1.4-million-electron-volt gamma ray from inelastic scattering. Aluminum and silicon each give a 1.8-Mev line spectrum with a half-life of 2.3 minutes in the activation spectrum, but silicon gives

the same prompt gamma ray from inelastic scattering. Iron is characterized by a 0.84-Mev prompt gamma ray and a fairly strong high-energy capture gamma ray. The conclusions of such a qualitative analysis will, of course, be tempered by considerations of natural background, neutron interactions in the detector, detector resolution, and stability of the energy calibration of the detector system. Nevertheless, it should be apparent that the use of spectra of all three types obtained in a combination experiment will yield more conclusive information than any single experiment.

In order to differentiate among the three rock types on the basis of gamma-ray spectral data, it is necessary to obtain quantitative results. It appears that the best way to achieve this is by measuring ratios among amounts of elements present. Referring to Table 1, we see that the ratios of oxygen to iron and to magnesium change uniformly across the rock types. From Fig. 2 it is evident that these two ratios could be determined from the inelastic spectrum alone. It would not be necessary to know the ratio of fast-neutron to thermal-neutron flux. However, this ratio may be available if the three spectra are taken in a single measurement. For example, if iron is fairly abundant, then a comparison of the 0.84-Mev inelastic gamma ray and the 7.6-Mev capture gamma ray, corrected for differences in detection efficiency, would yield an average fast-to-thermal ratio. This ratio would be needed if the capture spectrum should indicate the presence of strongly absorbing trace elements and if quantitative analysis of these elements is to be attempted.

Die-Away Measurement

In addition to the three spectral measurements, the die-away experiment offers some unique advantages. It can be performed at the same time as the spectral experiments to give the decay constant of the die-away of capture gamma rays. After each neutron burst, the intensity of capture gamma rays is measured as a function of time. After data have been collected for many neutron bursts, a curve of neutron intensity as a function of time is obtained. The curve will be similar to those labeled "capture" in Fig. 1.

The die-away decay constant λ depends upon two processes: absorption

Table 1. Estimates of concentrations (percent by weight) of elements in lunar maria and terrae. [From Palm and Strom (1)]

Element	Type of rock					
	Acidic		Basaltic		Aerolitic	
O	47	-52	43	-46	33	-44
Si	31	-38	21	-24	17	-25
Al	5	-10	3.5-	9	1	-6
Fe	1	-6	6.5-10		12	-22
Mg	0.1	-2	3	-14	14	-18
Ca	.1	-3	5	-8	1	-7
Na	.2	-4	1	-2.5	0.6	-0.8
K	1	-5	0.2-	1.5	.1	-0.2
Ni					.1	-1.7
S					.2	-2
H	0.07-	0.2	.1-	1	.03-	0.1

of thermal neutrons, and leakage of thermal neutrons out of the surface. We may approximate λ by the expression

$$\lambda = \nu\Sigma + DB^2$$

where ν is the thermal neutron velocity, Σ is the macroscopic absorption cross section, D is the diffusion coefficient, and B^2 is the effective "buckling."

The product DB^2 is not very sensitive to rock type and is approximately constant with a given orientation. The velocity will depend on the surface temperature at the time of the measurement. Σ is given by the formula

$$\Sigma = \rho \sum_i \frac{w_i \sigma_{ai}}{A_i}$$

where ρ is the density, and w_i , σ_{ai} , and A_i are, respectively, the weight fraction, microscopic absorption cross section, and atomic weight of the i th type nucleus. Using average values of w_i from Table 1, we have calculated Σ/ρ for the three rock types as shown in the second column in Table 2. There are differences of the order of 25 percent in the exponent of the function to be measured. In order to utilize these differences, ρ and DB^2 must be known. An estimate of the density may be made available by soft-landing experiments. If not, the thermal die-away results will have to be interpreted in terms of various assumptions about the surface density. The leakage term can

Table 2. Die-away parameters. For definition of symbols, see text.

Crystal rock type	Neutrons		R
	Thermal $\sum_i \frac{w_i \sigma_{ai}}{A_i}$	Epithermal $\sum_i \frac{w_i \xi_i \sigma_{si}}{A_i}$	
Acidic	0.0065	0.0070	1.08
Basaltic	.0086	.0142	1.65
Aerolitic	.0106	.0051	0.481

be obtained from laboratory experiments under realistic conditions and may be verified by theoretical calculations. Under these circumstances, a measurement of λ will determine the quantity

$$\nu \sum_i \frac{w_i \sigma_{ai}}{A_i}$$

Practically all absorption cross sections vary as ν^{-1} , so the dependence of ν on surface temperature is compensated for by an inverse dependence of σ_{ai} . In other words, one does not need to know the actual surface temperature.

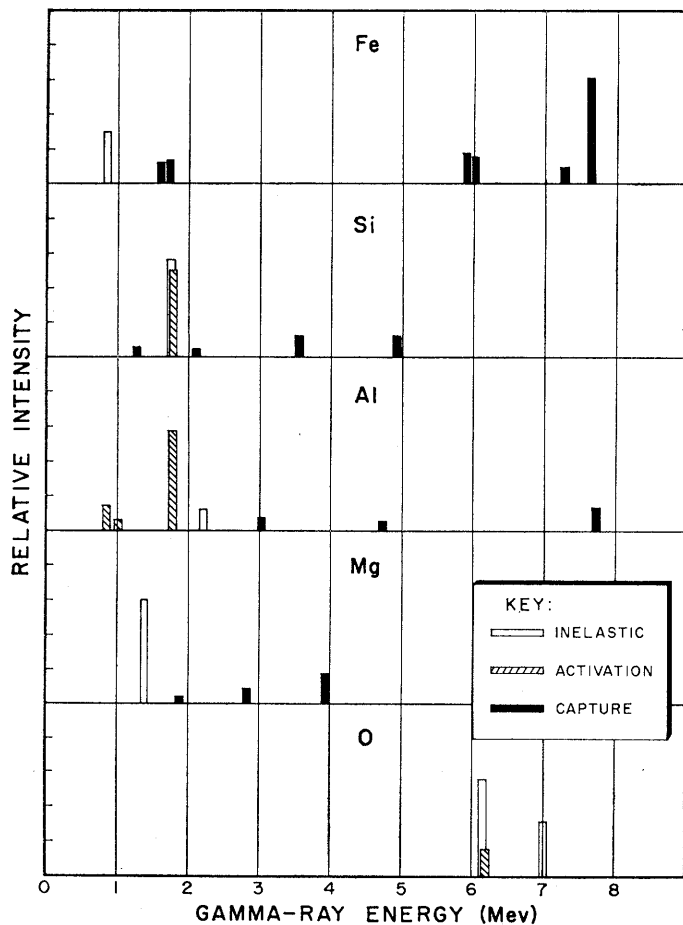


Fig. 2 (left). Spectral diagram for combination neutron experiment showing the effect of layering.

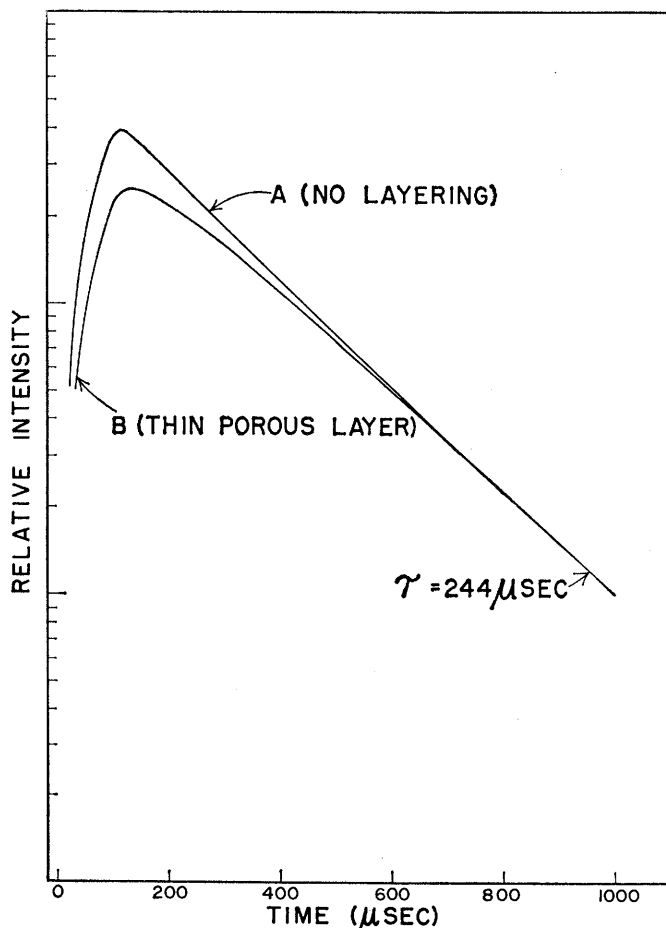


Fig. 3 (right). Theoretical neutron die-away calculation

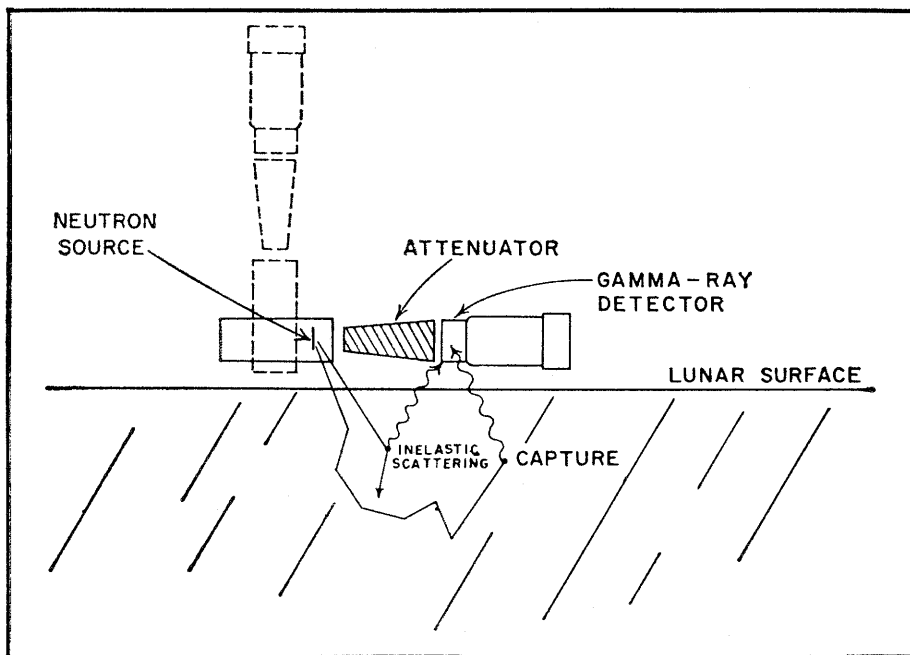


Fig. 4. Geometrical arrangements of the neutron probe with respect to the lunar surface.

The die-away experiment may also be used to measure hydrogen content, and thereby to provide an indication of the presence of water. This capability results from the fact that hydrogen dominates in the process of slowing down the fast neutrons from the source to thermal energy.

If decay of epithermal capture gamma rays can be observed, then the decay constant should be dependent primarily on hydrogen content and provide an independent indication of rock type. The epithermal decay constant is related to the quantity

$$\sum_i \frac{w_i \xi_i \sigma_{si}}{A_i}$$

where ξ_i and σ_{si} are, respectively, the average logarithmic energy decrement per collision and the average scattering cross section for fast neutrons for the i th type nucleus. Values for the above quantity are given in Table 2. As with the thermal decay constant, a good range of values is indicated for the three types of rock. Even though the amounts of hydrogen present are small, the contribution to the decay constant from hydrogen ranges from 45 percent for aerolitic to 85 percent for basaltic rock. Comments made above on ρ and DB^2 apply also to measurement of epithermal die-away.

If both the thermal and epithermal decay constants can be determined, then a sensitive measure of the rock type

which is independent of density may be obtained. To see this we write

$$\lambda_{th} = v_{th} \Sigma_{th} + (DB^2)_{th}$$

$$\lambda_{epi} = v_{epi} \Sigma_{epi} + (DB^2)_{epi}$$

Rearranging, we have

$$\Sigma_{th} = \left(\frac{\lambda - DB^2}{v} \right)_{th}$$

$$\Sigma_{epi} = \left(\frac{\lambda - DB^2}{v} \right)_{epi}$$

All quantities on the right side of these two equations are known. Define R as

$$R = \left(\frac{\lambda - DB^2}{v} \right)_{epi} / \left(\frac{\lambda - DB^2}{v} \right)_{th} = \Sigma_{epi} / \Sigma_{th}$$

Using the expressions for the Σ 's, we see that

$$R = \sum_i \frac{w_i \xi_i \sigma_{si}}{A_i} / \sum_i \frac{w_i \sigma_{at}}{A_i}$$

R , which is independent of ρ , is given in Table 2. It shows larger changes for the three rock types than either the thermal or epithermal parameters alone.

The die-away technique appears to offer some distinct advantages. The results of the measurement will be unaffected by changes in source output from burst to burst, or by a shift in the gain of the gamma-ray spectrometer. A definite physical parameter, Σ , is measured. One benefit of this fact may be seen in the following argument. The

results of measurements of inelastic, capture, and activation gamma rays may permit a definite decision to be made in favor of one of the three rock types. However, it is unlikely that the density of the rock can also be deduced from these measurements alone. On the other hand, the thermal die-away experiment yields a value of Σ , knowledge of the rock type gives

$$\sum_i \frac{w_i \sigma_{at}}{A_i},$$

and the ratio of these yields ρ . An additional advantage of measuring a definite physical parameter is that it provides a useful correlating quantity for results obtained at different locations.

If layering exists with a distinct interface no deeper than about 20 centimeters, the thermal die-away curve may exhibit a characteristic two-component behavior. In Fig. 3 we show two theoretical die-away curves to illustrate this point. These results were obtained through the use of a computer code which numerically solves the space- and time-dependent three-group neutron diffusion equations (7). We have assumed a point source of fast neutrons on the surface of a semi-infinite medium and have plotted the thermal-neutron time distribution at a point on the surface 30 centimeters from the source. Curve A was calculated by assuming the entire medium to be dense acidic rock. A value of 0.0065, as given in Table 2, was used for Σ_{th}/ρ , and the density was assumed to be 2.50 grams per cubic centimeter. Curve B was calculated by assuming that a porous layer of acidic rock with density 1.25 grams per cubic centimeter extends to a depth of 10 centimeters and dense acidic rock lies below. The curves have been normalized in the range 800 to 1000 μ sec. Both cases yield the same value of 244 μ sec for the asymptotic mean lifetime. The early part of the decay, however, is different for the two curves. After about 200 μ sec, curve A always has positive curvature on the semilog plot, whereas curve B has negative curvature. A time decay curve similar to B should be obtained whenever a thin porous layer overlies a dense rock.

Neutron Probe and Orientation

Figure 4 shows a simplified diagram of the apparatus for the combination neutron experiment. The source, attenuator

ator, and detector are arranged in a straight line, which may be either parallel or perpendicular to the surface to be analyzed. A small probe of this type, with a miniature pulsed accelerator neutron source, has been built (9, 10). No preparation of samples is required; the instrument is simply deployed on the surface in either a horizontal or vertical orientation. The horizontal orientation has the advantage of being easier to achieve remotely than vertical orientation.

For an actual space mission the neutron source will have to be compact, rugged, and reliable. This can be achieved with a miniature accelerator using the deuterium-tritium reaction to produce 14-Mev neutrons. The neutron output required will depend on the orientation of the probe and on the pulse-rate capabilities of the multichannel analyzer. An analyzer having input pulse inspection and a positive means of rejecting pile-up pulses will make it possible to use higher neutron outputs, which are desirable for the activation

part of the combination neutron experiment. Such an analyzer would allow operation of the neutron source at an output of approximately 1 to 5×10^3 neutrons per pulse at a rate of about 200 to 1000 pulses per second. These operating conditions would be suitable for measurement of the prompt and capture spectra and for the die-away experiment. Good shielding of the detector from the intense burst of bremsstrahlung accompanying the production of fast neutrons in a portable neutron source is mandatory for the prompt-gamma-ray part of the experiment. For activation measurements a time-integrated flux of up to about 10^7 neutrons per second could be used if the neutron source could be operated in a second mode of higher output. The attenuator between the neutron source and gamma-ray detector should be 15 to 20 centimeters of copper, or the equivalent shielding of some other material. The gamma-ray detector most suitable would be a NaI(Tl) scintillation counter, about 7 centimeters in diameter and

7 centimeters long. The energy resolution of the detector for cesium-137 gamma rays should be 8 percent or better.

A multichannel pulse-height analyzer comparable to instruments in general laboratory use would be suitable for this experiment. It would require a magnetic-core memory capacity of 544 channels. This memory would be organized to provide for simultaneous storage of two pulse-height spectra of 256 channels each (prompt and capture gamma-ray spectra) and one 32-channel time spectrum for the neutron die-away measurement. The activation experiment will utilize one of the 256-channel portions after the source is turned off. The performance of the analog-to-digital converter would have to be comparable to that of present laboratory instruments. The high data-acquisition rates in an experiment of this type would necessitate pile-up rejection circuitry to prevent distortion of pulse-height information. Although no such instrument suitable for space flight is

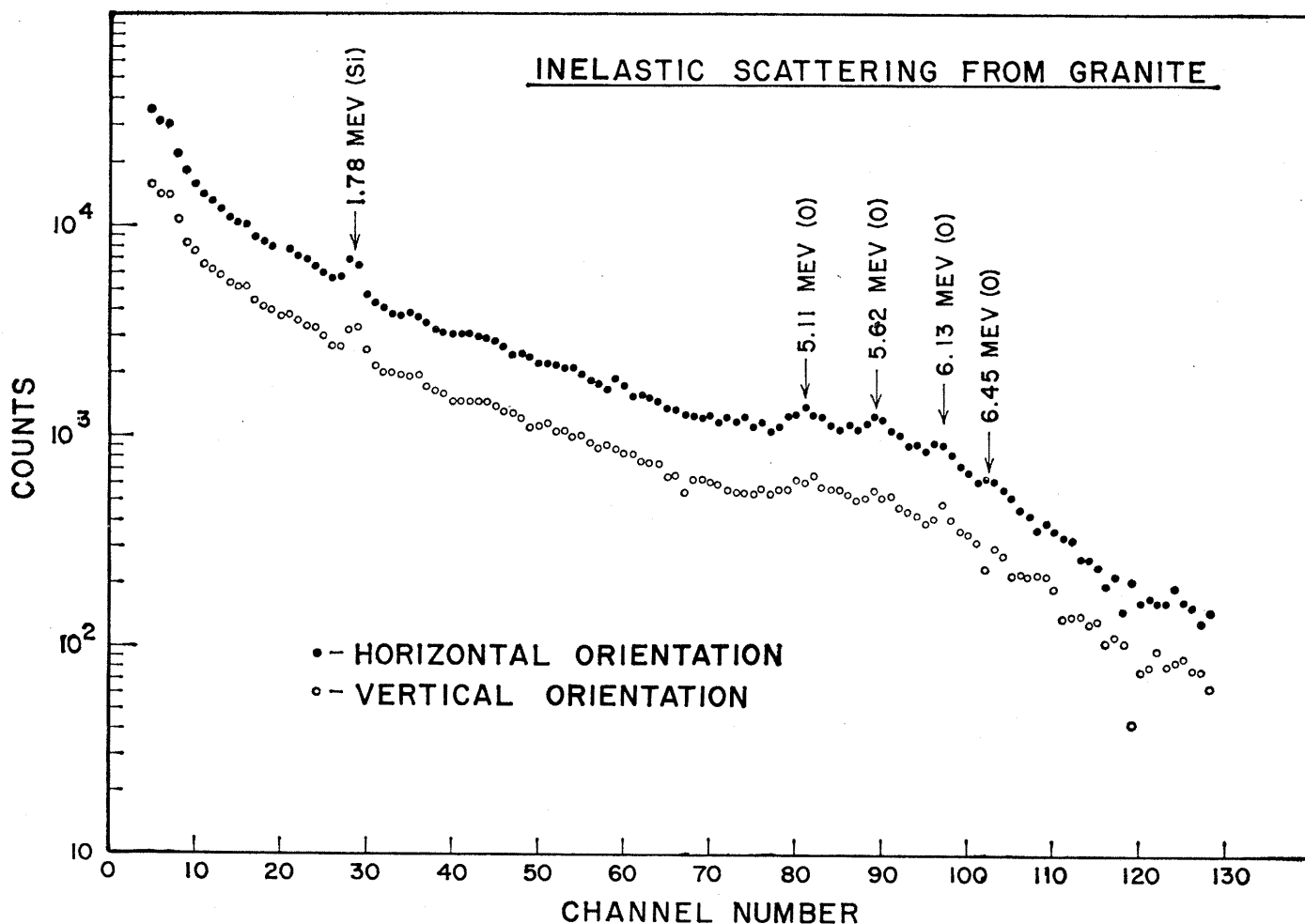


Fig. 5. Gamma-ray spectrum from inelastic scattering for horizontal and vertical probe orientation.

presently available, such equipment is under development.

As we envision it, the combination experiment would proceed as follows. After the neutron analysis probe is deployed on the lunar or planetary surface, and before the source is turned on, a background gamma-ray spectrum will be stored in one of the two 256-channel sections of the analyzer memory. These background data will be telemetered to earth or temporarily stored on magnetic tape for later transmission. The memory of the analyzer will then be cleared to zero, the neutron source turned on, and the inelastic scattering spectrum, the capture spectrum, and the die-away curve obtained. These will be routed to the proper por-

tions of the analyzer memory by timing and gating signals generated on the basis of a timing diagram such as that shown in Fig. 1. After a certain length of time (probably of the order of 30 minutes), the neutron source will be shut off and the contents of the analyzer memory telemetered to earth or temporarily stored on tape. The memory will again be cleared to zero, and a gamma-ray spectrum of radioactivity created by neutron activation will be obtained. If temporary storage on tape or telecommunication channels will permit, several activation spectra may be taken at different times after the source has been shut off, so that the decay of short-lived activities can be observed.

Experimental Results

We have performed several preliminary experiments which show the feasibility of the proposed combination experiment. Studies of the inelastic-scattering technique for remote chemical analysis of unknown materials have been reported (4, 9). We have performed an inelastic-scattering experiment in which we compared results obtained when the apparatus was vertically oriented with those obtained with a horizontal arrangement (14-Mev neutrons from a Van de Graaff accelerator were used). The arrangements shown in Fig. 4 were used on an array of granite blocks 48 centimeters square by 20 centimeters thick. The distance between the source and the detector was 27 centimeters, the attenuator was 14 centimeters of tungsten, and the gamma-ray detector was a NaI crystal, 5 centimeters in diameter by 5 centimeters long, on a Dumont 6363 photomultiplier. The analyzer was gated on only long enough to include the 5- μ sec fast neutron burst. The results of the experiment are shown in Fig. 5. The total neutron output in each run was 7×10^8 , and the integrated analyzer counting rate for each was about 1 count per 8 bursts. The curves have not been corrected for background, which amounts to about 25 percent for the horizontal orientation and 50 percent for the vertical. The 6.13-Mev oxygen gamma ray and the 1.78-Mev silicon gamma ray from inelastic scattering of fast neutrons are about equally well resolved from the two positions. The net counting rate is about three times higher with the horizontal orientation than with the vertical.

We next performed a neutron die-away experiment on a block of granite approximately 75 centimeters on each side, using a Philips neutron tube as the pulsed source. A 20-centimeter lead block served as the attenuator between the neutron source and a NaI detector, 5 centimeters in diameter by 5 centimeters long. These three units were approximately centered on the top face of the block in the horizontal arrangement shown in Fig. 4. For this experiment the neutron burst length was 5 μ sec, the 14-Mev neutron output was about 1×10^8 neutrons per burst, and the pulse repetition rate was 825 pulses per second. The time-decay data are shown in Fig. 6. Two runs were taken, one with 16- μ sec time channels and one with 1- μ sec channels. The solid

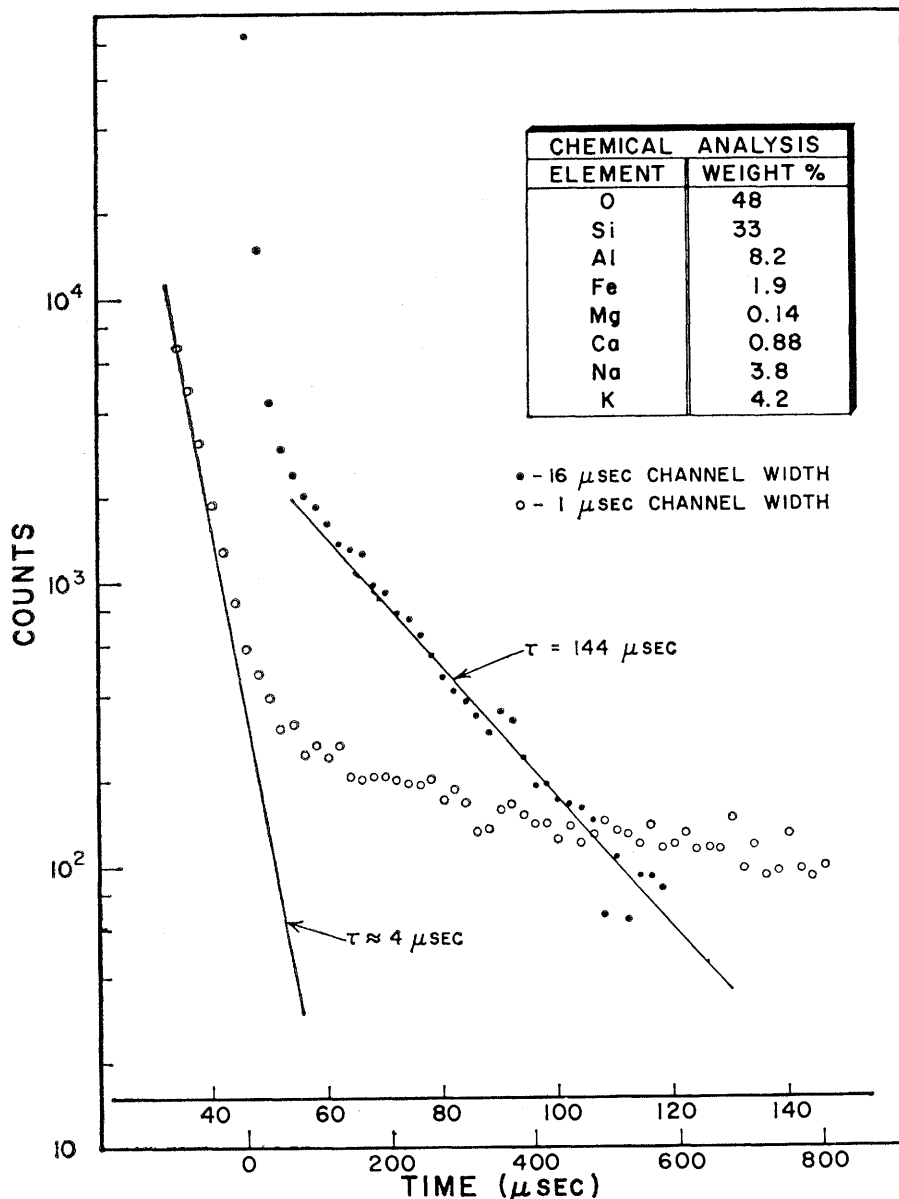


Fig. 6. Experimental die-away data for gamma rays from a granite block 75 by 75 by 75 centimeters.

circles show the 16- μ sec data corrected for background. The lower time scale applies to these data. Gamma rays from inelastic scattering are contained in the first channel beginning at time zero which includes the burst. After about 100 μ sec the decay appears to be exponential. The data after about 200 μ sec have been numerically fitted to a straight line by the method of Behrens (11), and a value of 144 μ sec obtained for the mean lifetime. The chemical analysis of the granite is very close to that of the average acidic rock for which the theoretical calculations of Fig. 3 were carried out. The large discrepancy between the experimental and theoretical asymptotic lifetimes is probably due to one or more of the following: (i) the granite block was not a semi-infinite medium, and considerable lateral leakage of neutrons occurred; (ii) strongly absorbing trace elements may have been present in the granite; (iii) diffusion theory, on which the calculations are based, is known to be inadequate at outer boundaries of a medium. These points need further investigation,

but the data show that a sufficient number of slow neutrons are produced within the block to permit the die-away measurement to be easily made.

The open circles show the 1- μ sec channel data corrected for background. The upper scale at the bottom of Fig. 6 is to be used with these data. A fast-decaying component is evident, with a lifetime of approximately 4 μ sec. We believe this short lifetime is due partly to hydrogen; however, no moisture analysis was performed on the rock.

A normal activation run was made by using the pulsed Van de Graaff source and the 48-centimeter-square by 20-centimeter-thick array of granite blocks with horizontal orientation. The neutron burst length was 5 μ sec, the time between bursts was 1200 μ sec, and the blocks were bombarded for 30 minutes with an output of about 1×10^7 neutrons per second, or a total of 1.8×10^{10} neutrons. A 1-minute count was begun 5 seconds after the end of neutron bombardment, and a 30-minute count was begun a few seconds after the end of the 1-minute

count. Essentially all of the 7.3-second N^{16} activity was counted in the 1-minute run. These results are labeled "normal" in Fig. 7. Note that the data points for the 1-minute count have been multiplied by 10.

In addition, we performed a different type of activation experiment using the same blocks, neutron burst length, and time between bursts, and the same orientation of the apparatus. In this technique, which might be called activation with cyclic counting, the multi-channel pulse-height analyzer is gated on during each irradiation cycle for an interval beginning after the capture gamma rays have died away and ending just before the next burst occurs. For example, the activation gate for the single large granite block would begin at about 1000 μ sec (see Fig. 6). A die-away measurement on the array of small granite blocks indicated very little capture radiation coming from this rather small system. We set an activation gate to begin 200 μ sec after the burst and end 100 μ sec before the next burst, giving a counting gate of 900 μ sec. The

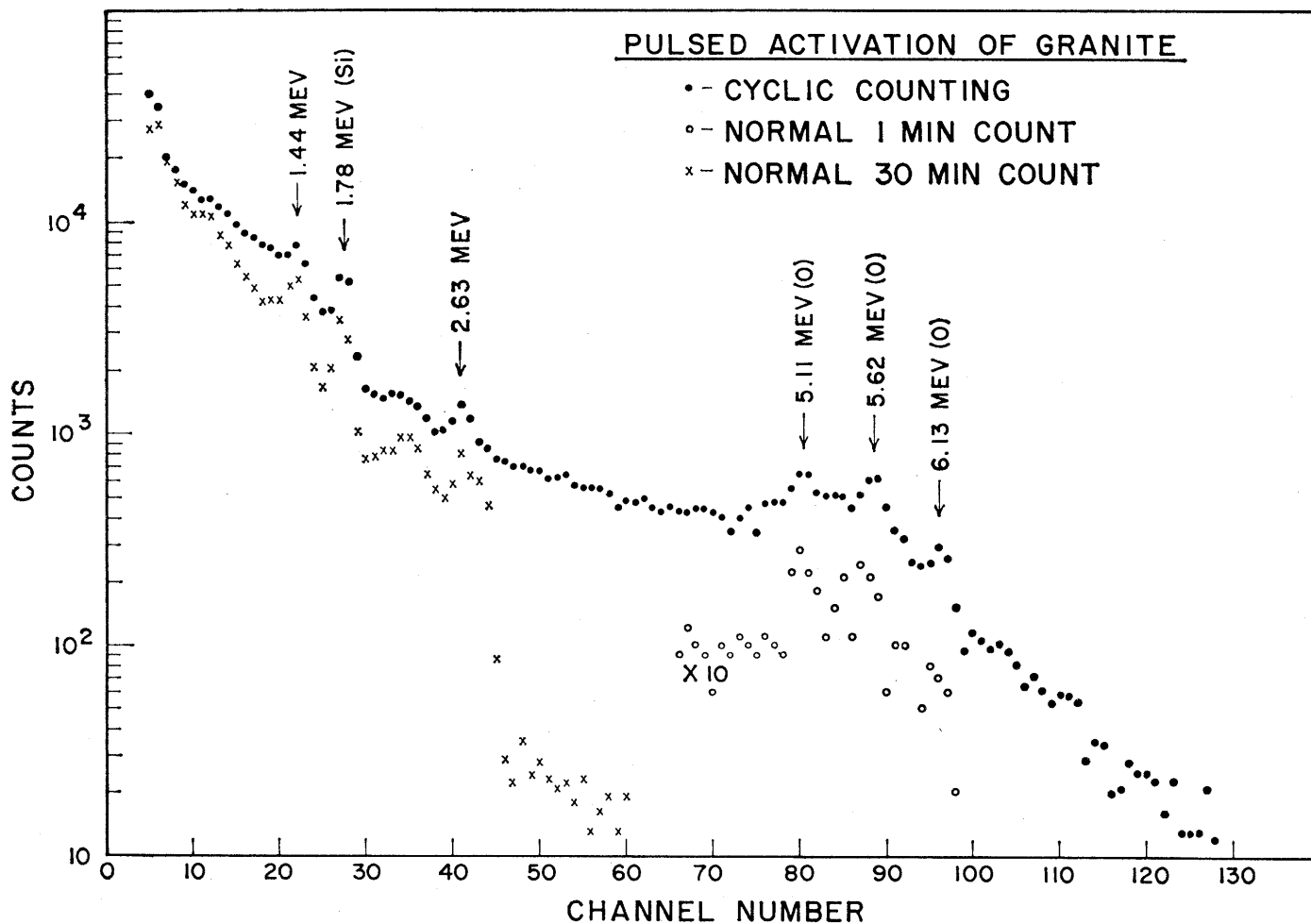


Fig. 7. Experimental comparison of pulsed activation with cyclic and with normal counting.

blocks were bombarded for 32 minutes with an output of about 0.16×10^7 neutrons per second, or a total of 0.31×10^{10} neutrons, with cyclic counting during the run. From the data, shown in Fig. 7, and the outputs quoted above, we see that pulsed cyclic activation is an improvement in counting rate over pulsed delayed activation by a factor of about 150 for oxygen detection and of about 9 for the low-energy portion of the spectrum. Thus pulsed cyclic activation is particularly appropriate for short-lived activities. The 6.13-Mev oxygen gamma ray and 1.78-Mev silicon gamma ray are prominent in Fig. 7. The 1.44- and 2.63-Mev gamma rays are attributed to natural radioactivity from potassium (1.46 Mev) and thorium (2.62 Mev), respectively. This explanation is supported by a spectrum, taken several days after bombardment, that showed the same two peaks.

A weakness of the cyclic activation method is that it cannot be used to determine half-lives much greater than the interval between fast neutron bursts. Further studies are needed to evaluate the possibilities of this method. Such studies would indicate whether cyclic

activation should be included as part of the proposed combination neutron-analysis experiment.

To compare fast-neutron activation of granite and basalt we used two-block arrays of each which were 10 centimeters thick, 17 centimeters wide, and 48 centimeters long. Each array was bombarded with 14-Mev neutrons from the Van de Graaff accelerator; the apparatus was oriented horizontally. The bombardments were carried out for 30 minutes, for a total output of 1.65×10^{10} neutrons for the granite run and 1.82×10^{10} neutrons for basalt. For each bombardment, a 30-minute count was taken after a 1-minute delay; the results are shown in Fig. 8. When the differences in neutron output are taken into account, the silicon content of the granite is higher than that of the basalt, as evidenced by the intensity of the 1.78-Mev gamma ray. Since granite is an acidic rock, this observation agrees with the estimates in Table 1. The gamma-ray lines at 1.38 and 2.75 Mev in basalt are attributed to Na^{24} produced by the fast neutron reaction $\text{Al}^{27}(n, \alpha)\text{Na}^{24}$. A die-away experiment showed no capture gamma rays. Hence, the

1.38- and 2.75-Mev gamma rays could not have been produced by thermal neutron capture in sodium. In the granite spectrum the 1.38- and 2.75-Mev peaks are partially obscured by the 1.44- and 2.63-Mev peaks mentioned previously.

Capture-gamma-ray studies aimed at lunar-surface analysis have been carried out with small samples and reactor sources of thermal neutrons (6). In our experiment on the large granite block, moderation of the fast neutrons from the source occurred in the block itself. The gamma-ray spectrum recorded in the time interval 40 to 540 μsec was dominated by the high-energy gamma rays from N^{16} produced by fast-neutron activation of oxygen. To fully evaluate the capture gamma ray as well as other parts of the combination neutron experiment, a larger volume of rock should be used. A block about 125 centimeters square and 60 centimeters thick should be adequate for such experiments.

A combined neutron-analysis experiment has distinct advantages for unmanned exploration of lunar and planetary surfaces. No preparation of sam-

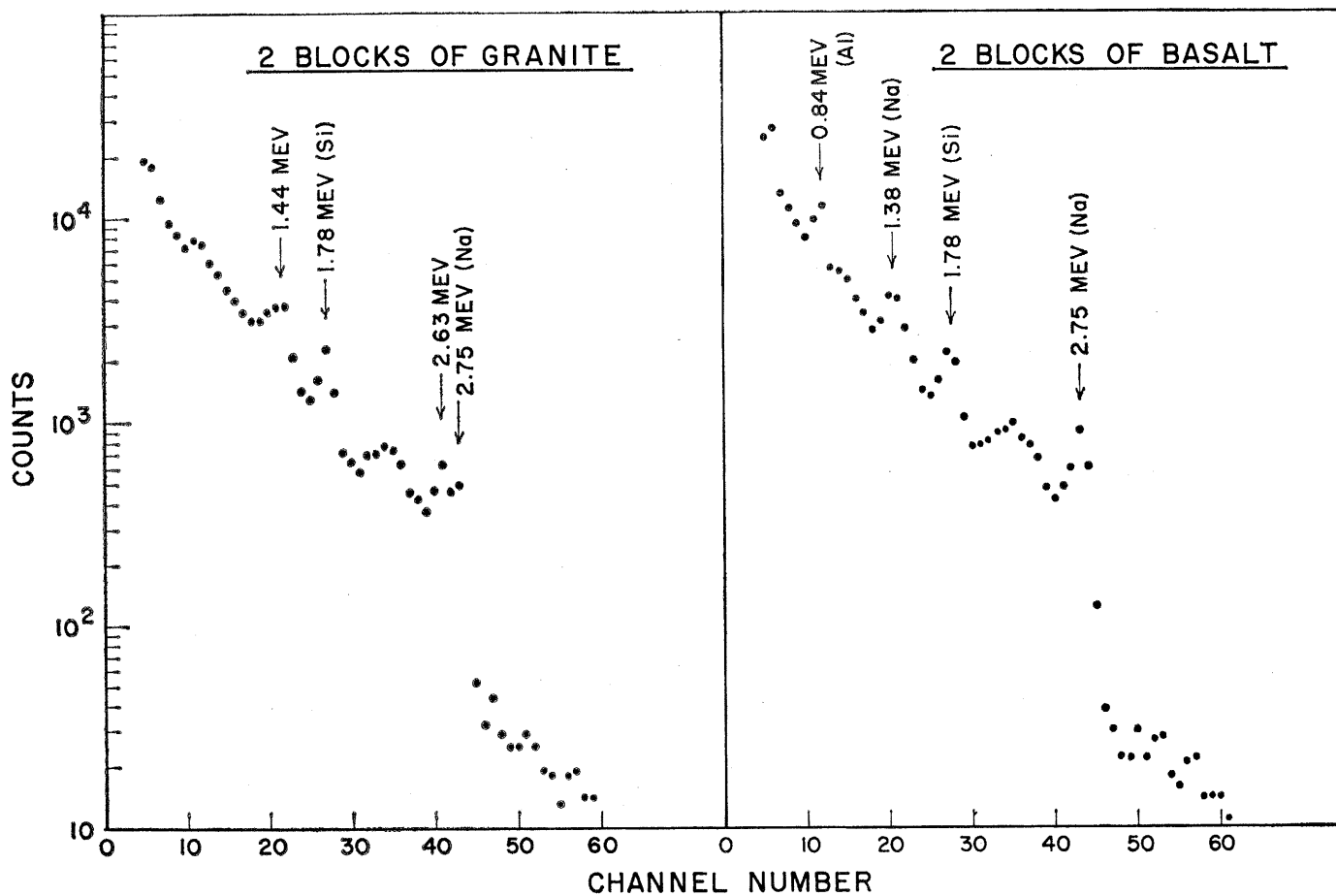


Fig. 8. Experimental comparison of activation of granite and basalt.

ples is required, and the success of the experiment does not depend on the orientation of the apparatus. Furthermore, the combined experiment can be performed with little more difficulty than a single type of neutron experiment. Further research is warranted to investigate the potentialities of this type of experiment more fully and in greater detail under realistic conditions. In particular, the errors and precision involved are not presently known, and these need to be established by suitable laboratory mock-up experiments.

References and Notes

1. A. Palm and R. G. Strom, "Research Report of Elemental Abundances of the Lunar Crust According to Recent Hypotheses," Series No. 3, Issue No. 5 (Space Sciences Laboratory, Univ. of California, Jan. 1962).
2. R. Monaghan, A. H. Youmans, R. A. Bergan, E. C. Hopkinson, *IEEE Inst. Electr. Electron. Eng. Trans. Nucl. Sci.* **10**, No. 1, 183 (1963).
3. J. I. Trombka and E. A. Metzger, *Analysis Instrumentation 1963* (Plenum, New York, 1963), pp. 237-250.
4. C. D. Schrader and R. J. Stinner, *J. Geophys. Res.* **66**, 1951 (1961).
5. M. P. Menon, "An Investigation of Computer-Coupled, Automatic, Remote Activation Analysis for Lunar Surface Analysis," Semi-annual Progress Report, May-November 1964 (Activation Analysis Research Laboratory, Texas A&M University, 1964).
6. R. C. Greenwood, J. H. Reed, R. D. Kolar, C. W. Terrell, *Trans. Am. Nucl. Soc.* **6**, 181 (June 1963).
7. W. R. Mills, Jr., L. S. Allen, R. L. Caldwell, G. N. Salaita, T. J. Gray, *Nucl. Sci. Eng.* **21**, 346 (1965).
8. A. H. Youmans, E. C. Hopkinson, R. A. Bergan, H. I. Oshry, *J. Petrol. Technol.* **16**, 319 (March 1964).
9. C. D. Schrader, J. A. Waggoner, J. H. Zenger, R. J. Stinner, *Am. Rocket Soc. J.* **32**, 631 (April 1962).
10. C. D. Schrader, J. A. Waggoner, A. E. Metzger, J. H. Zenger, *Nucleonics* **20**, No. 10, 67 (1962).
11. D. J. Behrens, "Some Notes on the Nature of Experiments, on the Statistics of Counting, and on the Fitting of Exponential Decay Curves to the Results of Counting Experiments," AERE T/R 629 (Atomic Energy Research Establishment, Harwell, Berks., England, 1951).

The Accessory Burrows of Digger Wasps

Like other manifestations of complex behavior, these are best understood through a comparative approach.

Howard E. Evans

Students of solitary wasps have long been intrigued by the varied and elaborate behavior patterns associated with nest closure and concealment. Many ground-nesting species disperse the mound of earth which accumulates at the entrance of the newly constructed nest. The dispersal movements assume many different forms and may be interspersed with digging movements or postponed until after the conclusion of digging. Many species prepare an "initial outer closure," scraping soil into the entrance either before or after leveling of the mound, or in the absence of mound-leveling behavior. Such species must reopen the nest entrance when they return to the nest and must restore the closure each time they leave. Subsequent temporary closures may be less complete than the initial one (for example, in *Bembix*), or they may actually be more complete (for example, in *Ammophila*). Certain wasps also prepare a "temporary inner closure" separating the cell from the burrow. When the nest is fully provisioned, the

wasp prepares a "final closure," which characteristically involves filling and packing the entire burrow as well as smoothing off the site of the entrance. Following final closure, some species pick up sticks, leaves, or other objects and place them over the site. Thus, with many digger wasps, the nest is effectively hidden from a human observer at all times when the wasp is not actually working at the nest entrance or entering or leaving (1).

It goes without saying that these wasps are able to find their own nests without hesitation, even when hundreds of such nests are scattered over an expanse of bare soil. While some digger wasps apparently require open nest entrances or markers in the immediate vicinity of the nest for orientation, bembicine wasps are able to locate their nests with the aid of points far distant from the nest, including, in some cases, the profile of the horizon as seen from a position facing the nest (2). There is no evidence that odor plays a role in nest finding.

A few days in the field suffice to convince one that such terms as *hiding* and *concealment* are not inappropriate—that is, that the biological role of these behavior patterns is in fact concealment from parasites and predators. We know that birds and mammals occasionally dig out the larvae of wasps, but this seems to be a rare occurrence. The major enemies of digger wasps are other insects, particularly members of two groups of flies and of two groups of parasitic wasps. The flies involved are bee flies (Bombyliidae) and miltoigrammine flies (Sarcophagidae, Miltoigramminae). Flies of both groups have short antennae and very large eyes and are believed to direct their activities with reference to the sight of the wasp or the open burrow. Bee flies, in fact, have been observed depositing their eggs in open holes of many kinds, including holes made with a pencil or, for that matter, eyelets in the shoes of the observer (3). The parasitic wasps include cuckoo wasps (Chrysididae) and "velvet ants" (Mutillidae). Members of both groups have well-developed antennae with which they tap the soil constantly during their search for nests of their hosts, and it seems certain that odor plays a role in nest finding in these wasps. However, the tarsal spines in members of these two groups are not nearly as fully developed as those of their hosts, and perhaps the thick closures often prevent these wasps from finding the cells of the nests of their hosts.

The author is curator of insects, Museum of Comparative Zoology, Harvard University, Cambridge, Massachusetts. This article is a condensation of material to be included in Dr. Evans' forthcoming book, *The Comparative Ethology and Evolution of the Sand Wasps*, to be published by Harvard University Press, and is published with permission of the President and Fellows of Harvard College.